GaN-Based Neutral-Point-Clamped Multi-Port DC-DC Converter

Xu, Ke; Echeverry, Jesse; Mackay, Laurens; Vahedi, Hani

DOI
10.1109/ICDCM63994.2025.11144652

Publication date
2025

Document Version
Final published version

Published in
2025 IEEE 7th International Conference on DC Microgrids, ICDCM 2025

GaN-based Neutral-point-clamped Multi-port DC-DC Converter

Ke Xu[1], *Member, IEEE*, Jesse Echeverry[2], Laurens Mackay[2], *Member, IEEE*, Hani Vahedi[1], *Senior Member, IEEE*

[1]Delft University of Technology, Department of Electrical Engineering, Delft, the Netherlands
[2]DC Opportunities R&D, Delft, the Netherlands

2025 IEEE Seventh International Conference on DC Microgrids (ICDCM) | 979-8-3315-1274-3/25/$31.00 ©2025 IEEE | DOI: 10.1109/ICDCM63994.2025.11144652

***Abstract*—This paper discusses the analysis and design of a multi-port DC-DC converter using Gallium Nitride transistors for a 350V bipolar DC grid application, which could be used as the first stage to interconnect a 350V bipolar DC grid and two electric vehicle batteries. The multi-port DC-DC converter is designed with a three-level neutral-point-clamped triple-active-bridge topology. The converter's parameters are selected on the basis of its performance characteristic and system specifications. Moreover, a simulation model is built to analyze the design. In the end, a prototype converter is built and the preliminary experimental results of it are shown and discussed.**

***Index Terms*—Three-level, triple-active bridge (TAB), gallium nitride (GaN), bipolar DC grid, EV charging.**

I. Introduction

Driven by environmental concerns and the predicted future shortage of fossil fuels, the energy transition to renewable-based electric systems is progressing rapidly. The increased penetration of renewable energy sources (RESs), energy storage systems (ESSs), and new types of load presents significant integration and operational challenges to electric systems. The growing adoption of these renewable energy components, along with advances in power electronics technology, highlights the advantages of DC grids in facilitating their integration in a direct and efficient manner [1], [2]. A bipolar DC grid can offer several advantages over conventional unipolar ones when properly regulated, such as greater availability, efficiency, retrofitting and flexibility [3].

The electrification of vehicles and thus the development of EV charging, is essential in the energy transition [4]. High-efficiency and high-density EV charging development is one of the keys to achieving the goal. In this context, Gallium Nitride (GaN), a wide-bandgap semiconductor material, has emerged as a promising solution for power electronics applications. It has higher electron mobility, saturation electron velocity, and breakdown electric field compared with silicon and silicon-carbon material [5], which leads to the possibility of its application in EV charging [6].

A multi-port DC-DC converter has been proposed and explored to meet the increasing demand for integrating renewable energy sources. It can interface multiple ports by only one conversion process, which reduces power conversion stages and thus decreases conversion losses. Moreover, a multi-port DC-DC converter can reduce the cost of material billing and increase power density [7]. A commonly used topology in DC grids to interconnect renewable energy sources to the grid is a triple active bridge (TAB) converter [8], [9], which is a natural extension of dual active bridge (DAB) converter. A high accuracy generalized average model (GAM) is generated for DAB converter analysis [10]. The modulation scheme of TAB converter is similar with DAB. The third port is not just an extension in terms of the performance characteristic, but also is highly coupled with the initial two ports. Fundamental frequency analysis (FCA), frequency-domain analysis (FDA) and generalised-harmonic-approximation (GHA) modelling method [11] are commonly used approaches for TAB converter analysis [12].

Considering the current state of GaN transistor technology, in order to integrate the GaN transistor into a 350V bipolar DC grid application, a multilevel topology is required. To utilize the advantage of GaN technology and multi-port converter, a three-level multi-port topology shall be analyzed. Multi-level operation has advantages in providing redundant switching states and improving the harmonic distortion, thus ensuring an easy voltage balancing process and improving overall performance [13], [14]. In previous works, either a normal two-level TAB or a three-level DAB converter was analyzed and built [15], [16]. This work combines GaN transistors, three-level topology, and multi-port structure to conduct analysis.

This paper puts forward a GaN-based multi-port EV charger solution for a 350V bipolar DC grid. The first stage of the EV charger, a three-level triple-active bridge converter, is analyzed in detail: first, the configuration of the EV charger is introduced based on system specifications. Afterward, two modulation schemes of the three-level triple-active bridge converter are discussed. Moreover, a simulation model is built and its results are discussed. In the end, the prototype design and experimental results of preliminary test are shown.

II. Configuration

A multi-port EV charger used for interconnecting a 350V bipolar DC grid and two EV batteries should be capable of bidirectional power flow and provide galvanic isolation between the DC grid and EV batteries.

A multilevel topology shall be used for GaN transistors to block working voltage properly. A neutral-point-clamped

(NPC) topology is selected because it is mature and has a relatively low cost. It does not require a complex modulation scheme for voltage balancing or an additional flying capacitor. Moreover, a full-bridge structure is selected in order to provide less current stress on components and harmonic distortion. In order to simplify the control scheme and maintain soft switching at a wide range of multi-port converters, a second-stage converter is added to the EV charger to convert the voltage of the first stage into a wide range of voltage that matches major EV batteries. With the second-stage converter, the first-stage converter only has to output voltage around a fixed value, making it easier for the first-stage converter to realize soft switching.

The multi-port EV charger consisting of a TAB converter and an interleaved buck converter is shown in Fig.1. The rated power of this charger is 11kW with DC grid side's rated voltage at 700V and battery side's voltage ranging from 200V to 920V. The maximum current on the battery side is 20A. The TAB converter is directly connected to a bipolar DC grid and has a fixed voltage range at the DC link, which is around 1000V. Two interleaved buck converters are connected to the EV batteries of each port and used to step down the DC-link voltage to the voltage of batteries. V_{11} and V_{12} represent positive-to-neutral and neutral-to-negative voltage of a bipolar DC grid respectively. V_{b1} and V_{b2} represent the voltage of EV batteries. The first stage of the EV charger, a three-level neutral-point clamped triple active bridge (NPC TAB) converter, is analyzed in detail.

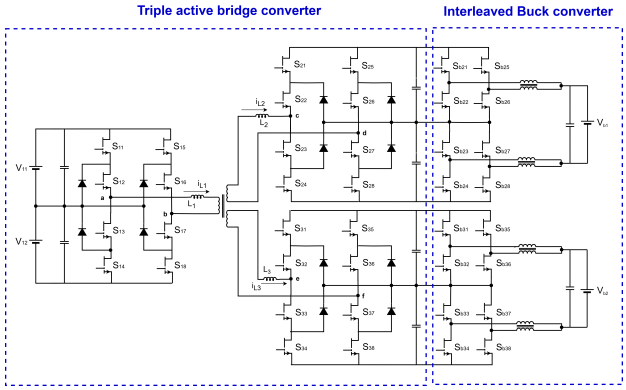

Fig. 1: Schematic of the multi-port EV charger

III. Phase-shift Control

Phase-shift control is used in the three-level NPC TAB converter. A three-level NPC full-bridge leg can output a maximum five-level voltage waveform depending on the modulation scheme (V_i,$\frac{V_i}{2}$,0,$-\frac{V_i}{2}$,$-V_i$). Similarly to the three-level NPC DAB converter, the modulation scheme of the three-level NPC TAB converter can be named based on the voltage level of the phase leg switched voltage output.

Fig.2 shows the voltage waveform of three ports under a three-level modulation scheme and a five-level modulation scheme. In the three-level waveform, $\alpha_1, \alpha_2, \alpha_3$ are the inner phase shift angles of three full bridges. φ_{12} and φ_{13} are phase-shift angles of primary-secondary side and primary-tertiary side. In the five-level waveform, $\alpha_1, \alpha_2, \alpha_3$ are the duty ratio angles of three full bridges. $\beta_1, \beta_2, \beta_3$ are the phase-shift angles between the bridge legs. φ_{12} and φ_{13} are defined as the same angles as in three-level modulation scheme.

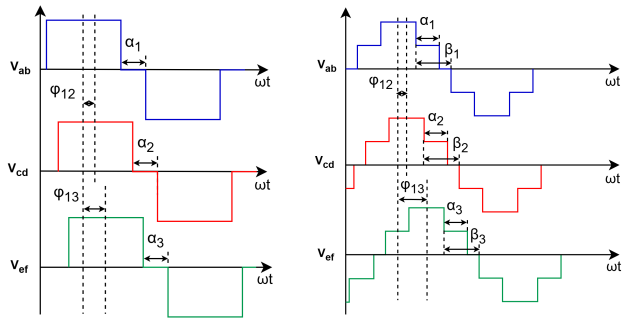

(a) (b)

Fig. 2: Phase leg switched voltages with (a)three-level modulation scheme (b)five-level modulation scheme

A. Three-level Operation

Fig.3 shows the switching sequence, phase leg switched voltage and inductor current of this modulation scheme. S_{11}, S_{14}, S_{15} and S_{18} are outer switches while S_{12}, S_{13}, S_{16} and S_{17} represent inner switches. The direction of current flow is defined as positive if it flows from the full bridge to the transformer.

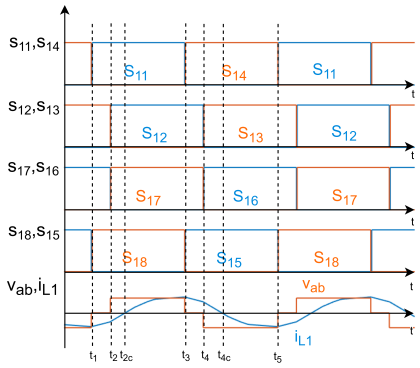

Fig. 3: Gate signals and other waveform of TAB with three-level modulation scheme

The switching sequence and power path of each subinterval are analyzed as follows:

- **(a)** $t_1 - t_2$**:** During this period, $S_{11}, S_{13}, S_{16}, S_{18}$ are in on-state while the inductor current flows from the transformer to the full bridge. Since S_{14} and S_{15} are in off-state, the current can only flow through two clamping diodes D_{13} and D_{16}. Because the current doesn't flow through any split capacitors, the phase leg switched voltage V_{ab} is 0.

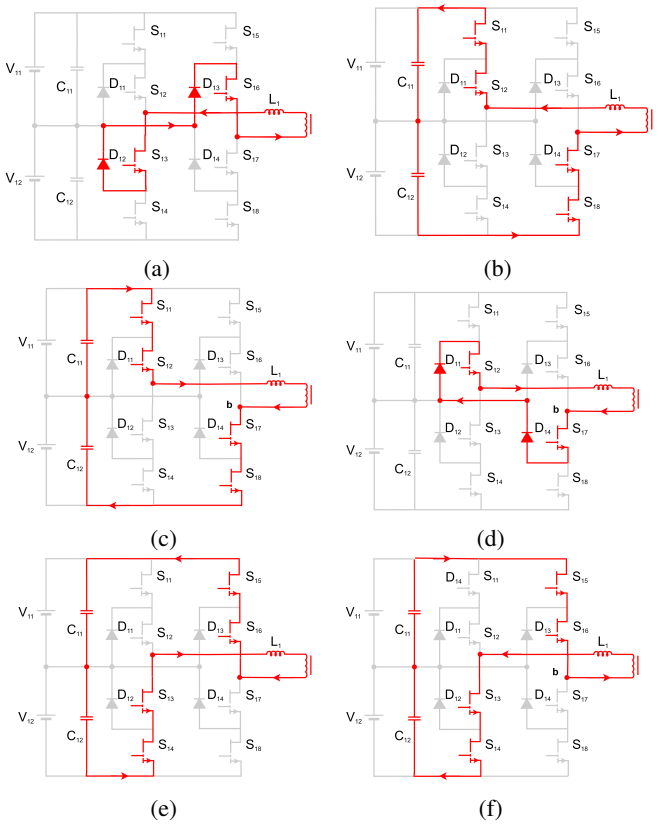

Fig. 4: Equivalent circuit model under three-level modulation scheme during various intervals (a)$t_1 - t_2$ (b)$t_2 - t_3$ (c)$t_3 - t_{3c}$ (d)$t_{3c} - t_4$ (e)$t_4 - t_5$ (f)$t_5 - t_6$

- **(b)** $t_2 - t_{2c}$**:** During this period, $S_{11}, S_{12}, S_{17}, S_{18}$ are in on-state while the inductor current flows negatively. So the current flows reversely through these switches. The phase leg switched voltage V_{ab} is full voltage of the DC bus V_1 during this subinterval.
- **(c)** $t_{2c} - t_3$**:** During this period, $S_{11}, S_{12}, S_{17}, S_{18}$ are in on-state while the inductor current flows positively. So the current flows through these switches. The phase leg switched voltage V_{ab} is full voltage of the DC bus V_1 during this subinterval.
- **(d)** $t_3 - t_4$**:** During this period, $S_{12}, S_{14}, S_{15}, S_{17}$ are in on-state while the inductor current flows positively. Since S_{11} and S_{18} are in off-state, the current can only flow through two clamping diodes D_{11} and D_{14}. Because the current doesn't flow through any split capacitor, the phase leg switched voltage V_{ab} is 0.
- **(e)** $t_4 - t_{4c}$**:** During this period, $S_{13}, S_{14}, S_{15}, S_{16}$ are in on-state while the inductor current flows positively. So the current flows through these switches. The phase leg switched voltage V_{ab} is full voltage of the DC bus V_1 during this subinterval.
- **(f)** $t_{4c} - t_5$**:** During this period, $S_{13}, S_{14}, S_{15}, S_{16}$ are in on-state while the inductor current flows negatively. So the current flows reversely through these switches. The phase leg switched voltage V_{ab} is full voltage of the DC bus V_1 during this subinterval.

B. Five-level Operation

Fig.5 shows the switching sequence, phase leg switched voltage, and current of this modulation scheme. S_{11}, S_{14}, S_{15} and S_{18} are outer switches while S_{12}, S_{13}, S_{16} and S_{17} represent inner switches.

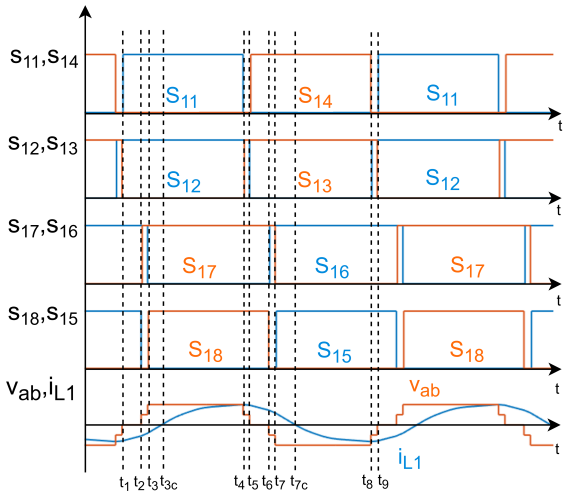

Fig. 5: Gate signals and other waveform of TAB with five-level modulation scheme

The switching sequence and power path of each subinterval are analyzed as follows:

- **(a)** $t_1 - t_2$**:** $S_{11}, S_{12}, S_{15}, S_{16}$ are in on-state while the inductor current flows from the transformer to the full bridge. Since the current doesn't flow through any split capacitor, the phase leg switched voltage V_{ab} is 0.
- **(b)** $t_2 - t_3$**:** $S_{11}, S_{12}, S_{16}, S_{17}$ are in on-state while the inductor current flows negatively. Since S_{15} is in off-state, the current flowing out from S_{11} cannot flow through it but flows through (charges) the split capacitor of the positive line C_{11} and clamping diode D_{13}. The phase leg switched voltage V_{ab} is equal to half the voltage of the DC bus $\frac{1}{2}V_1$ during this subinterval.
- **(c)** $t_3 - t_{3c}$**:** $S_{11}, S_{12}, S_{17}, S_{18}$ are in on-state while the inductor current flows negatively. Thus, the current flows from the source to the drain pin through all these switches. Since the current flows through (charges) two split capacitors, the phase leg switched voltage V_{ab} is equal to the full voltage of the DC bus V_1 during this subinterval.
- **(d)** $t_{3c} - t_4$**:** $S_{11}, S_{12}, S_{17}, S_{18}$ are in on-state while the inductor current flows positively. The two split capacitors are discharged. The phase leg switched voltage V_{ab} still equals the full voltage of the DC bus V_1 during this subinterval.
- **(e)** $t_4 - t_5$**:** $S_{12}, S_{13}, S_{17}, S_{18}$ are in on-state while the inductor current flows positively. Since S_{11} is in off-state,

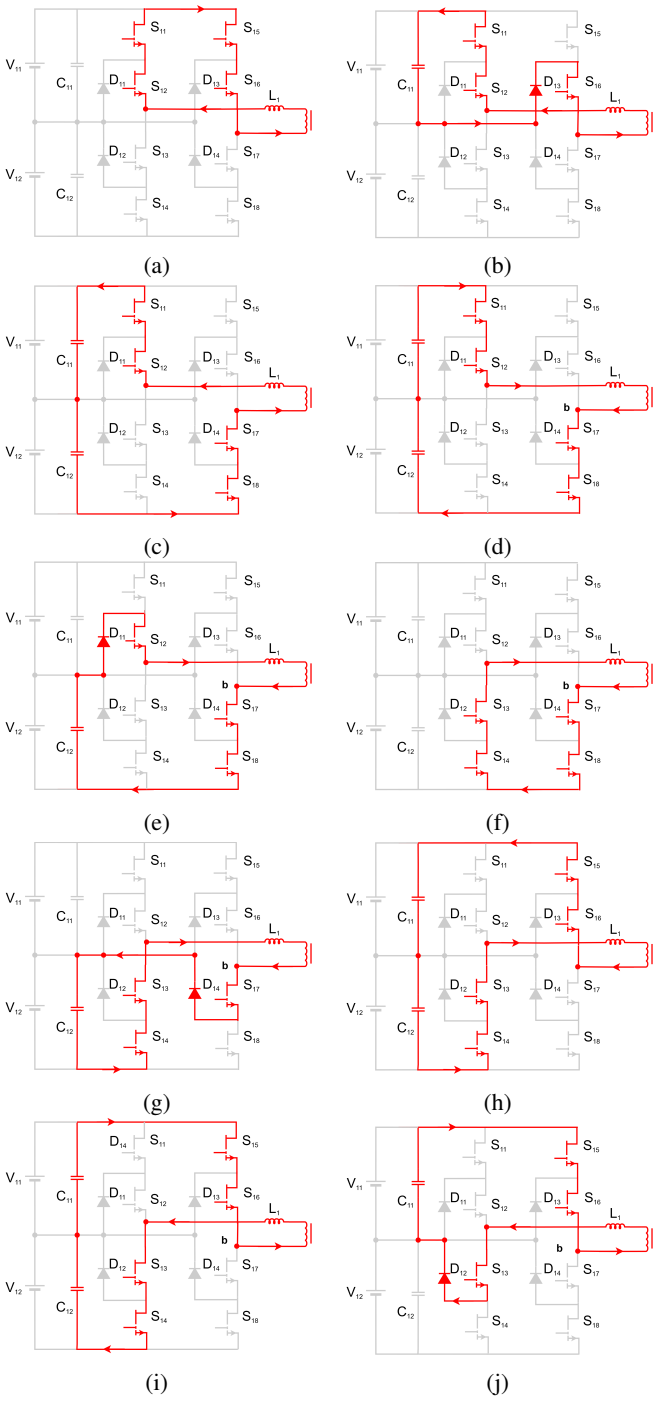

Fig. 6: Equivalent circuit model under five-level modulation scheme during various intervals (a)t_1-t_2 (b)t_2-t_3 (c)t_3-t_{3c} (d)$t_{3c}-t_4$ (e)t_4-t_5 (f)t_5-t_6 (g)t_6-t_7 (h)t_7-t_{7c} (i)$t_{7c}-t_8$ (j)t_8-t_9

the current flowing out from S_{18} cannot flow through it but flows through (discharges) the split capacitor of the negative line C_{12} and the clamping diode D_{11}. The phase leg switched voltage V_{ab} is V_{12}, which equals to half voltage of the DC bus $\frac{1}{2}V_1$ during this subinterval.

- **(f)** t_5-t_6**:** $S_{13}, S_{14}, S_{17}, S_{18}$ are in on-state while the inductor current flows positively. Since the current doesn't flow through any split capacitor, the phase leg switched voltage V_{ab} is 0.
- **(g)** t_6-t_7**:** $S_{13}, S_{14}, S_{16}, S_{17}$ are in on-state while the inductor current flows positively. Since S_{15} is in off-state, the current flows through (charges) the split capacitor of the negative line C_{12} and clamping diode D_{14}. The phase leg switched voltage V_{ab} is the full voltage of the DC bus $\frac{1}{2}V_1$ during this subinterval.
- **(h)** t_7-t_{7c}**:** $S_{13}, S_{14}, S_{15}, S_{16}$ are in on-state while the inductor current flows positively. Thus, the current flows from the source to the drain pin through all these switches. Since the current flows through (charges) two split capacitors, the phase leg switched voltage V_{ab} is equal to the full voltage of the DC bus V_1 during this subinterval.
- **(i)** $t_{7c}-t_8$**:** $S_{13}, S_{14}, S_{15}, S_{16}$ are in on-state while the inductor current flows negatively. The two split capacitors are discharged. The phase leg switched voltage V_{ab} still equals the full voltage of the DC bus V_1 during this subinterval.
- **(j)** t_8-t_9**:** $S_{12}, S_{13}, S_{15}, S_{16}$ are in on-state while the inductor current flows negatively. Since S_{14} is in off-state, the current flows through (discharges) the split capacitor of the positive line C_{11} and clamping diode D_{12}. The phase leg switched voltage V_{ab} is equal to half voltage of the DC bus $\frac{1}{2}V_1$ during this subinterval.

IV. Simulation

Based on the system specifications, the parameters of the converter are chosen and shown in Table I. The transformer turns ratio is selected to have the DC port voltage ratio close to unity. The inductance values are selected based on the rated transmission power between different ports.

TABLE I: Parameters of the simulated converter

Parameter	Symbol	Value
Input voltage	V_{11}, V_{12}	350V
DC-link voltage	V_{dc1}, V_{dc2}	1000V
Transformer turns ratio	n	$\frac{2}{3}$
Series inductance of port 1	L_1	11.98 μH
Series inductance of port 2	L_2	28.04 μH
Series inductance of port 3	L_3	28.04 μH
Switching frequency	f_{sw}	200 kHz
Grid side split capacitors	C_1, C_2	60 μF
Battery side split capacitors	$C_{o1}, C_{o2}, C_{o3}, C_{o4}$	50 μF

A simulation model of the three-level neutral-point clamped triple active bridge converter was built in PLECS. The converter model is simulated with both three-level and five-level modulation schemes.

Fig.7 shows the phase leg switched voltage and inductor current of each port of the converter under three-level opera-

tion with two 5.5 kW equal loads at battery sides. At steady state, the inner phase shift angle is 0.1π. Since the converter operates at equal loads, the secondary-to-primary and tertiary-to-primary phase shift angle are both 0.23π.

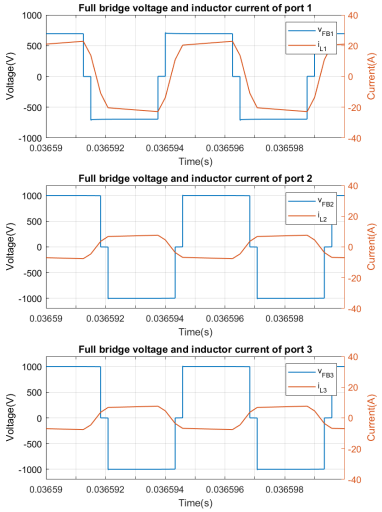

Fig. 7: Simulation results of three-level operation with equal loads at 5.5 kW

Fig.8 shows the phase leg switched voltage and inductor current of the converter with one load at 11 kW on one of the battery sides. At steady state, the inner phase shift angle is 0.1π. The secondary-to-primary phase shift angle is 0.38π.

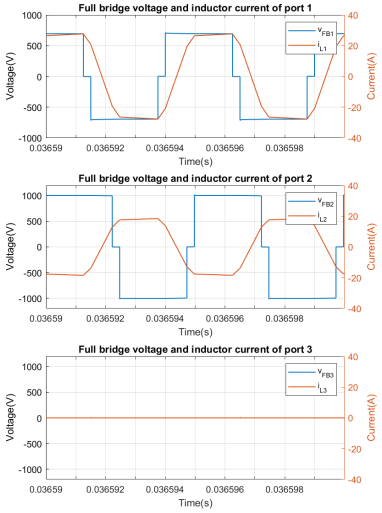

Fig. 8: Simulation results of three-level operation with full load at 11 kW on one port

Fig.9 shows the phase leg switched voltage and inductor current of each port of the converter with five-level operation with two 5.5 kW equal loads at battery sides. At steady state, the duty ratio angle is 0.1π, and the bridge phase shift angle is 0.2π. Since the converter operates at equal loads, the secondary-to-primary and tertiary-to-primary phase shift angles are both 0.33π.

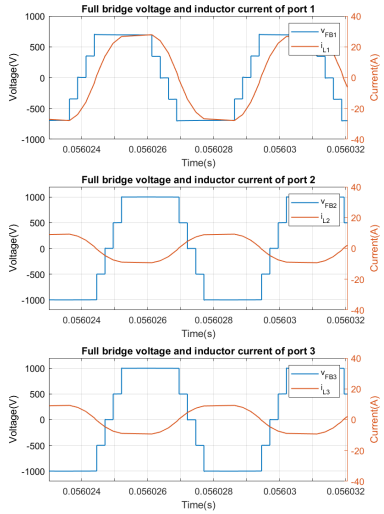

Fig. 9: Simulation results of five-level operation with equal loads at 5.5 kW

Fig.10 shows the phase leg switched voltage and inductor current of the converter with one load at 11 kW on one of the battery sides. At steady state, the duty cycle angle is 0.05π, and the inner phase shift angle is 0.1π. The secondary-to-primary phase shift angle is 0.41π.

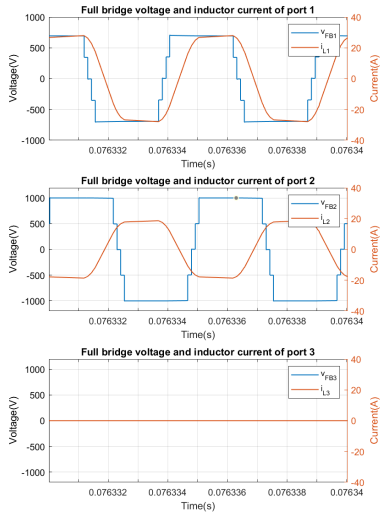

Fig. 10: Simulation results of five-level operation with full load at 11 kW on one port

V. Experimental Results

To verify the design presented in the previous section, a three-level NPC TAB converter has been built. The testing setup is shown in Fig.11. Two high voltage DC power supplies are used to simulate a DC grid and a DC link, respectively.

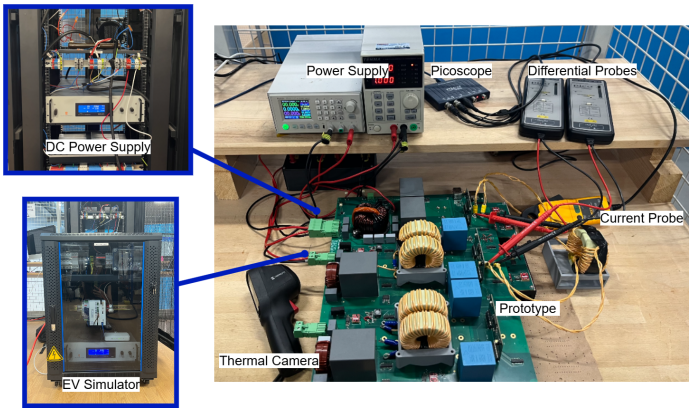

Fig. 11: Testing setup

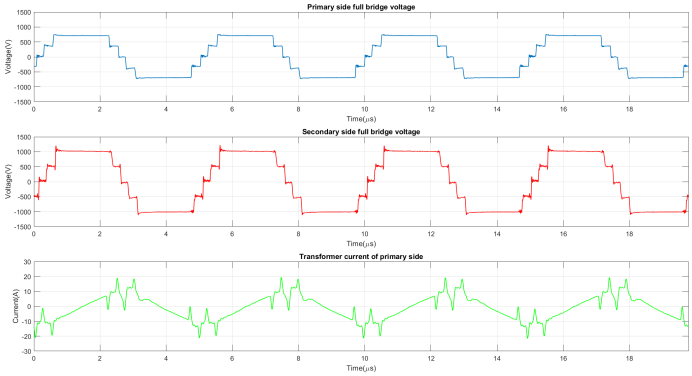

Fig. 12: Waveform of phase leg switched voltage and inductor current operating with two stages

A preliminary test with a single output port under open-loop control is conducted first. The operation point of the five-level operation is $V_{in} = 700V$, $V_{dc} = 1000V$, $\alpha = 0.1\pi$, $\beta = 0.2\pi$ and $\phi_{12} = 0.05\pi$. Fig.12 shows the waveforms of the phase leg switched voltage on primary and secondary sides as well as the inductor current on primary side. It can be seen that the phase leg switched voltage on both sides are five-level waveform with the set phase angles. The RMS value of the inductor current on the primary side is 8.52 A. For the input voltage of 700 V and an output voltage of 1000 V with the control variables, an output power of 1202 W can be realized. More experimental tests are being conducted and will be shown in the upcoming publication.

VI. Conclusion

In conclusion, a three-level neutral-point clamped triple-active-bridge converter used for a GaN-based multi-port EV charger is analyzed. The switching schemes with three-level and five-level operation are introduced on the basis of state analysis. Then, the parameters of the converter are selected based on the system specifications and its performance characteristic. In addition, a simulation model is built and the results are discussed. In the end, a prototype converter is built to verify the design and the results of the preliminary test are shown and discussed.

References

[1] G. P. Adam, T. K. Vrana, R. Li, P. Li, G. Burt, and S. Finney, "Review of technologies for dc grids – power conversion, flow control and protection," *IEEE Transactions on Power Delivery*, vol. 31, no. 3, pp. 919–933, 2016.

[2] E. Rodriguez-Diaz, F. Chen, J. C. Vasquez, J. M. Guerrero, R. Burgos, and D. Boroyevich, "Voltage-level selection of future two-level lvdc distribution grids: A compromise between grid compatibiliy, safety, and efficiency," *IEEE Electrification Magazine*, vol. 4, no. 2, pp. 20–28, 2016.

[3] S. Rivera, R. L. F., S. Kouro, T. Dragičević, and B. Wu, "Bipolar dc power conversion: State-of-the-art and emerging technologies," *IEEE Journal of Emerging and Selected Topics in Power Electronics*, vol. 9, pp. 1192–1204, Apr. 2021.

[4] H. Vahedi, M.-A. Forget, and P. Ibrahim, "Electric vehicle battery charger." https://patents.google.com/patent/US10759287B2/en, Sep 2020. U.S. Patent 10,759,287 B2.

[5] A. Udabe, I. Baraia-Etxaburu, and D. G. Diez, "Gallium nitride power devices: A state of the art review," *IEEE Access*, vol. 11, pp. 48628–48650, 2023.

[6] O. Bay, M. T. Tran, M. E. Baghdadi, S. Chakraborty, and O. Hegazy, "A comprehensive review of gan-based bi-directional on-board charger topologies and modulation methods," *Energies*, vol. 16, no. 8, p. 3433, 2023.

[7] A. Shekhar, G. C. R. Mouli, S. Bandyopadhyay, and P. Bauer, "Electric vehicle charging with multi-port converter based integration in dc trolley-bus network," in *2021 IEEE 19th International Power Electronics and Motion Control Conference (PEMC)*, pp. 250–255, 2021.

[8] M. Neubert, A. Gorodnichev, J. Gottschlich, and R. W. De Doncker, "Performance analysis of a triple-active bridge converter for interconnection of future dc-grids," in *2016 IEEE Energy Conversion Congress and Exposition (ECCE)*, pp. 1–8, 2016.

[9] N. Naseem and H. Cha, "Triple-active-bridge converter with automatic voltage balancing for bipolar dc distribution," *IEEE Transactions on Power Electronics*, vol. 37, no. 7, pp. 8640–8648, 2022.

[10] R. S. Deshmukh, P. Bauer, and H. Vahedi, "High-accuracy generalized average model of dual active bridge converters," *IEEE Open Journal of Power Electronics*, vol. 5, pp. 452–460, 2024.

[11] S. Zhang, J. Zhang, H. Zhang, Y. Wang, Y. Zhang, W. Zhang, and X. Zhang, "Analysis and experimentation of the quad-u variable inductor for power electronics applications," *IET Power Electronics*, vol. 12, no. 2, pp. 149–157, 2019.

[12] P. Koohi, A. J. Watson, J. C. Clare, T. B. Soeiro, and P. W. Wheeler, "A survey on multi-active bridge dc-dc converters: Power flow decoupling techniques, applications, and challenges," *Energies*, vol. 16, no. 16, p. 5927, 2023.

[13] H. Vahedi, M. Sharifzadeh, and K. Al-Haddad, "Topology and control analysis of single-dc-source five-level packed u-cell inverter (puc5)," in *IECON 2017 - 43rd Annual Conference of the IEEE Industrial Electronics Society*, pp. 8691–8696, 2017.

[14] D. Liu, Y. Wang, F. Deng, and Z. Chen, "Triple-phase-shift modulation strategy for diode-clamped full-bridge three-level isolated dc/dc converter," *IEEE Access*, vol. 8, pp. 2750–2759, 2020.

[15] L. Jin, B. Liu, and S. Duan, "Zvs operation range analysis of three-level dual active bridge dc-dc converter with phase-shift control," in *2017 IEEE Applied Power Electronics Conference and Exposition (APEC)*, pp. 362–366, 2017.

[16] H.-J. Byun, J.-M. Park, J. Yi, and C.-Y. Won, "Zero-voltage-switching analysis model of the triple-active-bridge converter," *Energies*, vol. 16, no. 23, p. 7763, 2023.